UDC 621.791.75:621.7.01

Denys Molochkov — PhD, Senior Lecturer, Department of Integrated Technologies of Electronic Devices, National University Zaporizhzhia Polytechnic, Zaporizhzhia, Ukraine, *e-mail: molochkov@zp.edu.ua*, ORCID: 0000-0002-9030-5371

Kyrylo Krasnoselsky — PhD student of the Department of Integrated Welding Technologies and Structural Modeling, National University Zaporizhzhia Polytechnic, Zaporizhzhia, Ukraine, *e-mail: kvkras@gmail.com*, ORCID: 0009-0006-5251-9076

SHIELDING GAS OXIDATION EFFECTS ON GEOMETRY AND ENERGETICS IN WIRE ARC DEPOSITION OF HIGH-STRENGTH STEEL

Purpose. *To establish the regularities of the influence of carbon dioxide concentration (0-100% CO_2) in an argon-based shielding mixture on the external macrogeometry (width, height, waviness) and energetic parameters of low-heat-input thin-wall formation from high-strength low-alloy (HSLA) MoNiVa steel using robotic Cold Metal Transfer (CMT) additive manufacturing.*

Research methods. *The studies were conducted using a robotic system with a Fronius TPSi power source (CMT mode, WFS = 2.0 m/min, TS = 35 cm/min). To eliminate subjective errors and analyze the stochastic macrogeometry, a computer vision method (OpenCV) based on pixel-by-pixel integration of optical scans (600 DPI, absolute error of 0.045 mm) was developed. Synchronizing geometric metrics with high-frequency (10 Hz) data logging of arc energetic parameters allowed for the evaluation of Volumetric Energy Density (VED).*

Results. *A fundamental scale effect was observed during thin-wall deposition. Monogas environments proved technologically unviable: 100% argon induced severe internal porosity due to molten pool viscosity and rapid freezing, while 100 % CO_2 caused spatial meandering, hydrodynamic collapse, and a catastrophic 45 % loss of cross-sectional area. An exceptionally stable technological window was identified strictly within 5–18% CO_2, where the coefficient of variation (CV) for the width was minimized (1.30–1.87%) and a proportional bead form factor was maintained.*

Scientific novelty. *For the first time, a thermohydrodynamic "scale effect" in WAAM of complex HSLA steels is formalized, proving that under low-heat-input conditions, active gas additions do not improve wetting but rather trigger rapid crystallization and oxide barrier formation. The "energy paradox" of the process is mathematically proven: despite the 100% CO_2 mode having the lowest linear heat input (205.5 J/mm) due to synergic current suppression, it requires the highest Volumetric Energy Density (2.09 kJ/cm³) owing to critical mass transfer deterioration.*

Practical value. *The identified technological window (5-18% CO_2) and the formalized energy balance for MoNiVa thin-wall structures serve as a ready-to-use foundation for minimizing geometric defects and maximizing energy efficiency in production. The developed machine vision algorithm is suitable for implementation in closed-loop WAAM control systems for predictive real-time parameter adjustment.*

Key words*: Wire Arc Additive Manufacturing, WAAM, Cold Metal Transfer, CMT, high-strength steel, MoNiVa, shielding gas, volumetric energy density, computer vision.*

Introduction

Wire Arc Additive Manufacturing (WAAM) is currently considered one of the most promising areas of metal 3D printing for large-scale objects tailored to the needs of the aerospace and heavy engineering industries. Its main advantages are high deposition rates, relatively low equipment costs, and the ability to use standard commercial welding wires. Of particular interest to the industry is the printing of parts from high-strength low-alloy (HSLA) steels, particularly those alloyed with molybdenum, nickel, and vanadium (MoNiVa system), which provide a unique combination of strength, toughness, and cold resistance.

However, the main drawback hindering the mass adoption of WAAM is the low dimensional accuracy and significant waviness of the side surfaces of the deposited walls. Since the process relies on free-form deposition, controlling the final dimensions of the part comes down to managing the hydrodynamics of the liquid weld pool. Deviations from the specified geometry require significant allowances for subsequent machining, which negates the economic benefits of the additive approach.

Problem statement

Unlike traditional welding, in WAAM, the bead shape is formed exclusively as a result of the evolution of the liquid metal pool under the influence of surface tension forces, viscous friction, and electrodynamic forces. Traditionally, kinematic parameters such as wire feed speed (WFS) and travel speed (TS) are used to control the geometry. The shielding gas is mostly considered a passive element for isolating the molten pool. However, changing its composition, in particular by adding active carbon dioxide (CO_2), alters the oxidation potential of the plasma and the

DOI 10.15588/1607-6885-2026-2-10

rheology of the molten pool, making it a fully-fledged independent tool for influencing shape formation, which remains understudied for steels with complex alloying systems.

Analysis of research and publications

The current state of development of additive technologies shows that the product geometry in WAAM is determined by the evolution of the metal pool under a moving heat source. Unlike processes with a strictly localized molten pool of small volume (e.g., laser powder bed fusion), shape accuracy in arc deposition must be considered as a complex problem of unsteady thermohydrodynamics with a free surface [1, 2]. The final bead shape results from the interaction of surface tension forces, viscous friction, gravity, droplet transfer momentum, and the overall thermal state of the molten pool [3-5]. Most studies prove that the key factors of geometric stability are heat input, deposition strategy, and the metal transfer algorithm [6]. However, the shielding gas is often still considered primarily as a passive technological parameter to ensure arc stability and protection from the atmosphere [7]. In recent years, the paradigm has been changing. Studies show that the gas environment should be considered an active shape control tool [8, 9]. Changing the gas composition affects not only the electrical and spatial characteristics of the arc discharge but also the surface state of the pool, the nature of convective flows, and the lifetime of the liquid phase. The fundamental basis for this approach was formed in studies of weld pool physics, which proved that Marangoni thermocapillary flows have a decisive influence on the deposition geometry [3, 4]. The magnitude and direction of these flows are determined by the sign and modulus of the surface tension temperature gradient. When using pure argon, the temperature gradient is negative, which initiates centrifugal molten pool flows from the center of the pool to its edges, resulting in relatively wide but shallow penetration. However, the addition of carbon dioxide is accompanied by its dissociation in the arc and the supply of surface-active oxygen to the liquid metal. As proven in classical works, even minor additions of active gas turn the surface tension gradient positive, initiating powerful centripetal flows that pull the molten pool toward the center and downwards, radically changing the macrogeometry and heat redistribution [3, 4]. Specifically for WAAM, the impact of gas mixtures has become the subject of empirical research only recently. In particular, studies for low-carbon and stainless steels demonstrate that changing the Ar/CO_2 ratio affects layer geometry, spatter, and surface roughness [10-14]. However, most of these studies analyze specific “ready-made” industrial mixtures rather than the systematic variation of the CO_2 fraction as a control parameter. Furthermore, they focus mostly on the materials science aspect (microstructure), bypassing mechanical interpretation through changes in the hydrodynamic field and energy efficiency. A specific challenge that currently remains ignored is the use of high-strength low-alloy (HSLA) steels in WAAM [15]. The application of complex alloyed steels (like MoNiVa) introduces an additional level of thermodynamic complexity. Alloying elements (especially molybdenum and vanadium) combined with an active gas can form complex refractory oxide films on the pool surface. Unlike simple silicate slags in ordinary steels, these films locally alter molten pool viscosity, acting as a mechanical barrier that restricts spreading and impairs interlayer wetting. Conversely, synergic algorithms of modern power sources (such as CMT) automatically change the current to compensate for gas dissociation, directly affecting the specific energy intensity of the process.

Furthermore, current theoretical frameworks of Marangoni thermocapillary flows in WAAM are predominantly based on high-heat-input regimes (thick-wall deposition) with a massive molten pool. The extrapolation of these rules to low-heat-input, thin-wall structures – where the pool volume is minimal and cooling rates are extreme – remains a critical gap in the literature. It is unclear whether the active gas additions can effectively trigger centripetal spreading before the small pool completely solidifies, especially for highly viscous alloys like MoNiVa.

Thus, the current scientific literature lacks an integrated approach combining a systematic analysis of the impact of the full spectrum of CO_2 concentrations (0–100 %) on macrogeometric stability and the energy balance of free-form deposition specifically for HSLA steels with complex molten pool rheology, which justifies the relevance of this study.

Purpose of the work

To establish the regularities of the influence of active carbon dioxide concentration (from 0% to 100%) in a mixture with argon on the macrogeometric stability, stochastic waviness, bead form factor, and specific volumetric energy density of low-heat-input thin-wall deposition of high-strength low-alloy MoNiVa steel using the robotic Cold Metal Transfer process.

Material and methods of research

To implement the experimental part of the work, a specialized robotic additive manufacturing complex was used. The kinematic system was based on a six-axis industrial manipulator Yaskawa MH1440. An inverter welding system, Fronius TPS500i, equipped with a hardware module for the CMT (Cold Metal Transfer) technology, was used as the power source. The choice of the CMT algorithm is due to its ability to minimize heat input through high-frequency reciprocating wire movement, which ensures mechanical droplet detachment at reduced short-circuit currents. This is critical for multi-layer 3D printing, where heat accumulation is the main cause of geometric wall degradation.

A solid welding wire with a diameter of 1.2 mm made of high-strength low-alloy (HSLA) steel with an Mn-Ni-

DOI 10.15588/1607-6885-2026-2-10

Mo-V alloying system was used. The presence of molybdenum and vanadium provides high strength but significantly changes the molten pool rheology, increasing its viscosity and tendency to form refractory oxide films in the presence of active gases. Deposition was carried out on S355 structural steel substrates.

Kinematic parameters were specifically optimized for low-heat-input thin-wall deposition: the wire feed speed (WFS) was set to 2.0 m/min, and the travel speed (TS) was reduced to 35 cm/min to stabilize pool hydrodynamics. The contact tip to work distance (CTWD) was 13 mm, and the torch tilt angle was 0 degrees. Shielding gas flow was maintained at 14 L/min. To investigate the oxidation potential, a gradient of gas mixtures from 100 % Ar to 100 % CO_2 was applied (including intermediate values of 5, 10, 15, 20, and 25 % CO_2). The process involved depositing 20 consecutive layers. To isolate the effect of thermal accumulation, a strict temperature control protocol was applied, ensuring an interpass temperature of 85±10 °C.

To eliminate subjective human factors in measuring the stochastic macrogeometry, a software package based on the OpenCV computer vision library (Python) was developed. Transverse macrosections were digitized using an optical scanner at 600 DPI (pixel size 0.0423 mm). The algorithm included Gaussian filtering, Otsu's adaptive binarization, and morphological closing. To eliminate edge effects, the algorithm automatically cropped 3.0 mm from the top and bottom bounds. For the stabilized central zone, the exact cross-sectional area (F) was calculated via pixel-by-pixel integration. Horizontal scanning determined the effective width, width extremes, standard deviation, and coefficient of variation (CV). Additionally, the algorithm calculated the geometrical Form Factor (φ) as the ratio of the average bead width to the average layer height. Hardware validation via a 10 mm reference standard confirmed an absolute error of 0.045 mm.

Energetic parameters (welding current I, arc voltage U) were recorded via the power source's built-in data logger at 10 Hz. A script extracted stationary process segments. Linear heat input (HI) and Volumetric Energy Density (VED, kJ/cm³) were subsequently calculated by integrating the energetic logs with the cross-sectional area extracted by the computer vision system.

Research results

Initial trials utilizing 100% argon shielding were deemed unsuccessful due to the active formation of internal porosity within the deposited bead. Consequently, pure argon was excluded from further systematic quantitative analysis, and the study focused on the gradient of CO_2-Ar mixtures.

Precision analysis of the cross-sectional macro-geometry revealed a strict, linear degradation of the thin-wall profiles as the CO_2 concentration increased (Figure 1). In the range of 5% to 25% CO_2, a gradual decrease in mass transfer was observed: the total wall height dropped from 33.78 mm to 29.93 mm, while the corresponding average layer height decreased from 1.689 mm to 1.496 mm. This was accompanied by a linear reduction in the cross-sectional area (F) from 178.73 mm² to 139.73 mm². However, the transition to 100 % CO_2 resulted in a catastrophic drop in geometric indicators (Table 1). The cross-sectional area plummeted to 98.22 mm², representing a 45% loss of material compared to the 5 % CO_2 baseline, while the total height collapsed to 20.36 mm.

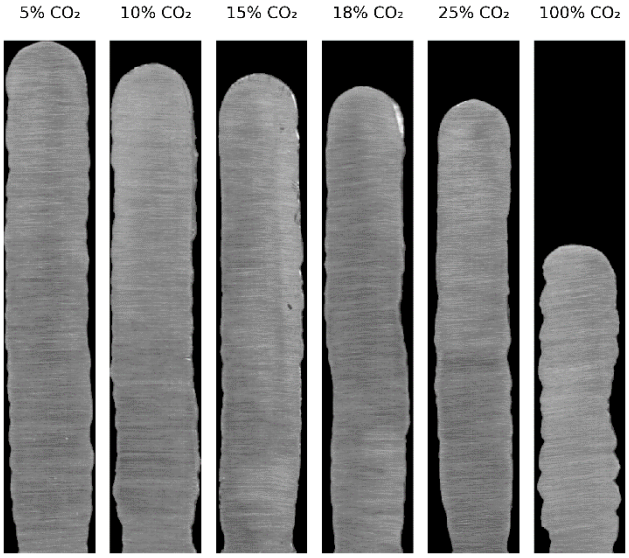

Figure 1. Macrogeometric profiles and calculated contours of the deposited MoNiVa walls as a function of CO_2 concentration

The average wall width exhibited a slightly different trend. The maximum width was recorded at 5–10 % CO_2 (5.46 mm). As the active gas fraction increased to 25 %, the bead gradually narrowed to 4.86 mm. Interestingly, at 100 % CO_2, the average width marginally increased to 4.96 mm, which, as subsequent visual analysis showed, was an artifact of severe spatial instability rather than uniform spreading. Statistical processing of the digitized bead masks provided an objective metric for assessing process stability. For the MoNiVa alloy system under thin-wall deposition parameters, an exceptionally stable technological window was identified in the range of 5–18 % CO_2. Within this zone, the coefficient of variation (CV) for the wall width was exceptionally low, ranging from 1.30 % to 1.87 % (Table 1), indicating near-perfect layer-by-layer reproducibility. A progressive collapse of stability occurred at higher CO_2 concentrations. The transition to pure carbon dioxide caused the CV to surge to 4.90 %. Macroscopic evaluation of the wall surface at 100 % CO_2 (Figure 2) demonstrated severe spatial meandering of every single bead. This longitudinal wandering led to a complete disruption of interlayer cohesion and the formation of deep interpass valleys, directly causing the aforementioned drop in total height and area.

DOI 10.15588/1607-6885-2026-2-10

Table 1 – Energetic and geometric indicators of the MoNiVa WAAM process (WFS = 2.0 m/min, TS = 35 cm/min)

Shielding gas mixture	I average, A	U average, V	P average, W	HI, J/mm	Cross-sectional area F, mm²	VED, kJ/cm³
5% CO_2	94,5	11,9	1508,5	258,6	178,73	1,45
10% CO_2	93,0	12,5	1540,4	264,1	171,13	1,54
15% CO_2	92,0	12,7	1543,2	264,5	163,20	1,62
18% CO_2	83,6	13,0	1398,3	239,7	152,59	1,57
25% CO_2	77,5	13,5	1335,8	229,0	139,73	1,64
100% CO_2	66,3	14,2	1198,5	205,5	98,22	2,09

Figure 2. Top view of the 100 % CO_2 deposited wall with severe spatial meandering

This degradation was further confirmed by the Form Factor anomaly (φ), calculated as the ratio of average width to average layer height. Within the 5–25 % CO_2 technological window, the Form Factor remained stable between 3.23 and 3.38. However, at 100 % CO_2, this indicator anomalously spiked to 4.87, serving as a mathematical reflection of the severe height collapse and erratic material deposition.

High-frequency data logging of the CMT power source parameters captured a pronounced electrical adaptation to the shielding gas effect on the process. While the wire feed speed was strictly fixed at 2.0 m/min, increasing the CO_2 concentration forced the equipment to elevate the average arc voltage from 11.9 V to 14.2 V. Simultaneously, the synergic control loop drastically suppressed the average welding current, which dropped from 94.5 A (at 5 % CO_2) to 66.3 A (at 100 % CO_2). This cyber-physical feedback directly impacted the energy balance. Contrary to expectations, the lowest linear heat input (HI) was recorded in the 100 % CO_2 environment (205.5 J/mm), whereas the optimal 10–15 % CO_2 mixtures generated approximately 264.1–264.5 J/mm. However, integrating the heat input with the cross-sectional area exposed an extreme peak in the Volumetric Energy Density (VED). The 100 % CO_2 mode required the highest amount of energy to build one cubic centimeter of metal –2.09 kJ/cm³ – compared to just 1.45 kJ/cm³ for the 5% CO_2 mixture.

Discussion

The complete failure to produce a defect-free thin wall in a 100 % argon atmosphere highlights the unique rheological challenges of HSLA steels. In pure argon, the absence of surface-active oxygen leads to a negative surface tension temperature gradient, driving centrifugal Marangoni flows. More critically, alloying elements such as molybdenum and nickel significantly increase the kinematic viscosity of the MoNiVa molten pool. In thin-wall deposition, the small pool volume cools and solidifies extremely fast. Without the “fluxing” and viscosity-reducing effects of an active gas, evolving gases (such as hydrogen) become trapped within the rapidly freezing viscous molten pool, inevitably resulting in the severe internal porosity observed during the initial trials.

A crucial finding of this study is the identified “scale effect” of heat input on the thermohydrodynamics of the molten pool. Previous theoretical frameworks regarding WAAM of carbon steels suggest that adding CO_2 improves wetting and spreading by generating active oxygen, which shifts the Marangoni flow from centrifugal to centripetal. However, our data on thin-wall structures (WFS = 2.0 m/min) proves the opposite. Under conditions of low overall heat input, the high energy demand for CO_2 dissociation drastically shortens the lifetime of the liquid phase. The molten pool “freezes” too rapidly, crystallizing before the centripetal thermocapillary flows can fully activate and redistribute the metal. Consequently, active gas additions on thin walls do not improve lateral spreading, leading instead to the observed linear degradation of the cross-sectional area. The catastrophic 45 % loss of cross-sectional area and the total loss of geometric stability (CV = 4.90 %) at 100% CO_2 are directly attributed to the complex chemical rheology of MoNiVa steel. In highly oxidizing environments, refractory oxide films of molybdenum and vanadium form instantaneously on the pool surface. Unlike simple silicate slags, these films act as a rigid mechanical shell that completely blocks interlayer wetting.

This oxide barrier, combined with the lowest heat input dictated by the CMT synergic loop, creates a molten pool with extreme viscosity. As a result, a phenomenon of severe longitudinal meandering occurs. The highly constricted arc column wanders across the pool surface searching for conductive pathways, but the viscous, oxide-covered metal cannot flow quickly enough to follow the heat source. This disconnect between the arc pressure and fluid flow tears the molten pool stream apart, triggering Rayleigh-Plateau hydrodynamic instability.

DOI 10.15588/1607-6885-2026-2-10

The recorded electrical logs – where voltage increased to 14.2 V and current plummeted to 66.3 A at 100% CO_2 – perfectly illustrate the thermodynamics of gas dissociation. The endothermic breakdown of polyatomic CO_2 molecules extracts significant heat from the arc, constricting its plasma column. To maintain a stable discharge against this cooling effect, the power source naturally elevates the voltage. To compensate for this voltage spike, the cyber-physical CMT algorithm drastically suppresses the average welding current along a strict inverse vector.

In standard GMAW processes, the current is intrinsically linked to the actual wire melting rate. We hypothesize that the synergic self-regulation of the CMT power source, by dropping the current so aggressively, effectively reduced the actual deposition rate despite the programmed WFS. This hidden drop in productivity, coupled with massive spatter caused by the arc deflecting off the oxide shell, fully explains the extreme metal deficit. Therefore, the anomalous jump of the Form Factor (φ) to 4.87 is not an indicator of a successfully flattened bead, but rather a mathematical proof of a "failed humping" effect: the spatial wandering and spatter prevented vertical buildup, leaving a disjointed track with a microscopic average layer height.

These interconnected phenomena culminate in the fundamental "energy paradox" of thin-wall WAAM. The 100% CO_2 mode exhibited the lowest linear heat input (HI = 205.5 J/mm). In traditional welding, lower heat input is often associated with better process control. However, in this free-form additive process, the constricted arc, impenetrable oxide barriers, and massive vaporization rendered the mode utterly unprofitable. The Volumetric Energy Density reached its maximum (VED = 2.09 kJ/cm³), meaning the highest amount of energy was wasted per cubic centimeter of successfully deposited metal.

In conclusion, this study establishes strict boundaries of technological robustness for precision thin-wall WAAM of complexly alloyed HSLA steels like MoNiVa. Monogas shielding is fundamentally unviable: 100% argon induces porosity due to high viscosity and gas trapping, while 100% CO_2 triggers severe meandering, spatter, and hydrodynamic collapse. The optimal balance between molten pool viscosity, surface tension, and heat input is strictly confined to a narrow technological window of 15–18 % CO_2, where perfect synergy between droplet transfer and mass assimilation is achieved.

Conclusions

This study establishes that the shielding gas oxidation potential is a critical factor governing the thermohydrodynamics of low-heat-input thin-wall WAAM for complex HSLA MoNiVa steels. A fundamental "scale effect" was identified, which inverses the typical influence of active shielding gases observed in massive depositions. Specifically, monogas environments proved technologically unviable for this alloy: 100 % argon induces severe internal porosity due to high molten pool viscosity and the rapid freezing of the small pool volume, whereas 100 % CO_2 triggers hydrodynamic collapse. The highly oxidizing environment leads to the formation of rigid, impenetrable Mo-V oxide films, manifesting as severe spatial meandering and a catastrophic 45% loss of cross-sectional area (dropping to 98.22 mm²).

Conversely, precision computer vision analysis statistically justified an exceptionally stable technological window strictly within the range of 5–18% CO_2. Within this gradient, the deposition achieves ideal layer-by-layer geometric reproducibility with minimal stochastic waviness, maintaining a coefficient of variation between 1.30 % and 1.87 % alongside a proportional and predictable bead form factor.

Furthermore, these geometric transformations are inextricably linked to the formalized "energy paradox" of the cyber-physical CMT process. To compensate for the endothermic dissociation in pure CO_2, the synergic loop drastically suppresses the average current to 66.3 A, resulting in the lowest linear heat input of 205.5 J/mm. However, due to massive material loss and spatter, this mode is actually the least energetically efficient, driving the Volumetric Energy Density to a maximum of 2.09 kJ/cm³. Ultimately, optimal energy efficiency (1.45–1.62 kJ/cm³) and stable mass transfer are achieved exclusively at 5–15 % CO_2, proving that gas chemistry and molten pool rheology, rather than electrical power alone, fundamentally dictate the geometric and economic viability of the thin-wall WAAM process.

References

1. Zhang, H., Li, R., Liu, J., Wang, K., Qiu, W., Shi, L., & et al. (2024). State-of-art review on the process-structure-properties-performance linkage in wire arc additive manufacturing. Virtual and Physical Prototyping, 19(1), e2390495. https://doi.org/10.1080/17452759.2024.2390495

2. Jafari, D., Vaneker, T. H. J., & Gibson, I. (2021). Wire and arc additive manufacturing: Opportunities and challenges to control the quality and accuracy of manufactured parts. Materials & Design, 202, 109471. https://doi.org/10.1016/j.matdes.2021.109471

3. Wang, Y., & Tsai, H. L. (2001). Effects of surface active elements on weld pool fluid flow and weld penetration in gas metal arc welding. Metallurgical and Materials Transactions B, 32, 501–515. https://doi.org/10.1007/s11663-001-0035-5

4. Lu, S., Fujii, H., & Nogi, K. (2004). Marangoni convection and weld shape variations in Ar-O_2 and Ar-CO2 shielded GTA welding. Materials Science and Engineering: A, 380(1-2), 290–297. https://doi.org/10.1016/j.msea.2004.05.057

5. Wu, F., Falch, K. V., Guo, D., English, P., Drakopoulos, M., & Mirihanage, W. (2020). Time evolved force domination in arc weld pools. Materials & Design, 190, 108534. https://doi.org/10.1016/j.matdes.2020.108534

6. Cunningham, C. R., Flynn, J. M., Shokrani, A., Dhokia, V., & Newman, S. T. (2018). Strategies and processes for high quality wire arc additive manufacturing. Additive Manufacturing, 22, 672–686. https://doi.org/10.1016/j.addma.2018.06.020

DOI 10.15588/1607-6885-2026-2-10

7. Kah, P., & Martikainen, J. (2013). Influence of shielding gases in the welding of metals. The International Journal of Advanced Manufacturing Technology, 64 (9–12), 1411–1421. https://doi.org/10.1007/s00170-012-4111-6

8. Teixeira, F. R., Jorge, V. L., Scotti, F. M., Siewert, E., & Scotti, A. (2024). A methodology for shielding-gas selection in wire arc additive manufacturing with stainless steel. Materials, 17(13), 3328. https://doi.org/10.3390/ma17133328

9. Silwal, B., Pudasaini, N., Roy, S., Murphy, A. B., Nycz, A., & Noakes, M. W. (2022). Altering the supply of shielding gases to fabricate distinct geometry in GMA additive manufacturing. Applied Sciences, 12(7), 3679. https://doi.org/10.3390/app12073679

10. Yamaguchi, M., Komata, R., Furumoto, T., Abe, S., & et al. (2022). Influence of metal transfer behavior under Ar and CO_2 shielding gases on geometry and surface roughness of single and multilayer structures in GMAW-based wire arc additive manufacturing of mild steel. The International Journal of Advanced Manufacturing Technology. https://doi.org/10.1007/s00170-021-08231-8

11. Kanishka, K., Acherjee, B., & et al. (2025). A study on the effect of shielding gases on the GMAW-WAAM process and performance of WAAM-deposited low-carbon steel. International Journal of Materials Research. https://doi.org/10.1515/ijmr-2024-0319

12. Akbarzadeh, E., Yurtışık, K., Gür, C. H., & et al. (2024). Influence of shielding gas on the microstructure and mechanical properties of duplex stainless steel in wire arc additive manufacturing. Metals and Materials International, 30(7), 1977–1996. https://doi.org/10.1007/s12540-023-01623-3

13. Marefat, F., Kapil, A., Banaee, S. A., Van Rymenant, P., & Sharma, A. (2023). Evaluating shielding gas-filler wire interaction in bi-metallic wire arc additive manufacturing (WAAM) of creep resistant steel-stainless steel for improved process stability and build quality. Journal of Manufacturing Processes, 88, 110–124. https://doi.org/10.1016/j.jmapro.2023.01.046

14. Yang, G., Deng, F., Zhou, S., Wu, B., Qin, L., & Zheng, J. (2022). Influence of shielding gas nitrogen content on the microstructure and mechanical properties of Cu-reinforced maraging steel fabricated by wire arc additive manufacturing. Materials Science and Engineering: A, 832, 142463. https://doi.org/10.1016/j.msea.2021.142463

15. Rodrigues, T. A., Duarte, V., Avila, J. A., Dias, M. R., Santos, T. G., & Oliveira, J. P. (2019). Wire and arc additive manufacturing of HSLA steel: Effect of thermal cycles on microstructure and mechanical properties. Additive Manufacturing, 27, 440–450. https://doi.org/10.1016/j.addma.2019.03.029

Received 15.04.2026
Accepted 24.04.2026
Published 07.05.2026

УДК 621.791.75:621.7.01

ВПЛИВ ОКИСЛЮВАЛЬНОЇ ДІЇ ЗАХИСНОГО ГАЗУ НА ГЕОМЕТРІЮ ТА ЕНЕРГЕТИКУ ДУГОВОГО 3D-ДРУКУ ВИСОКОМІЦНОЮ СТАЛЛЮ

Денис Молочков — доктор філософії, старший викладач кафедри інтегрованих технологій електронних засобів Національного університету «Запорізька політехніка», м. Запоріжжя, Україна *e-mail: molochkov@zp.edu.ua*, ORCID: 0000-0002-9030-5371

Кирило Красносельський — аспірант кафедри інтегрованих технологій зварювання та моделювання конструкцій Національного університету «Запорізька політехніка», м. Запоріжжя, Україна, *e-mail: kvkras@gmail.com*, ORCID: 0009-0006-5251-9076

Мета роботи. *Встановлення закономірностей впливу концентрації вуглекислого газу (0–100 % CO_2) у захисній суміші з аргоном на зовнішню макрогеометрію (ширину, висоту, хвилястість) та енергетичні показники процесу формування тонкостінних структур з низьким тепловкладенням із високоміцної низьколегованої сталі (HSLA) MoNiVa з використанням роботизованого адитивного виробництва за технологією CMT (Cold Metal Transfer).*

Методи дослідження. *Дослідження проводились із застосуванням роботизованого комплексу з джерелом живлення Fronius TPSi (режим CMT, швидкість подачі дроту 2,0 м/хв, швидкість зварювання 35 см/хв). Для усунення суб'єктивних похибок та аналізу стохастичної макрогеометрії розроблено метод комп'ютерного зору (OpenCV) на основі попіксельного інтегрування оптичних сканів (600 DPI, абсолютна похибка 0,045 мм). Синхронізація геометричних метрик з високочастотним (10 Гц) логуванням енергетичних параметрів дуги дозволила оцінити питому об'ємну енергію (VED).*

Отримані результати. *Під час тонкостінного наплавлення виявлено фундаментальний масштабний ефект. Використання моногазів виявилося технологічно недоцільним: 100% аргон провокує сильну внутрішню пористість через високу в'язкість розплаву та його швидке твердіння, тоді як 100 % CO_2 спричиняє просторове меандрування, гідродинамічний колапс та катастрофічну втрату 45 % площі поперечного перерізу. Визначено зону надвисокої технологічної стабільності в строгому діапазоні 5–18 % CO_2, де коефіцієнт варіації (CV) ширини досягає мінімуму (1,30–1,87 %) при збереженні пропорційного форм-фактора валика.*

DOI 10.15588/1607-6885-2026-2-10

Наукова новизна. *Вперше формалізовано термогідродинамічний «масштабний ефект» у WAAM-технології для складних HSLA сталей. Доведено, що в умовах низького тепловкладення додавання активного газу не покращує змочування, а навпаки, провокує швидку кристалізацію та утворення оксидних бар'єрів. Математично доведено «енергетичний парадокс» процесу: незважаючи на те, що режим 100 % CO_2 має найнижче лінійне тепловкладення (205,5 Дж/мм) завдяки синергетичному придушенню струму, він потребує найвищої питомої об'ємної енергії (2,09 кДж/см³) через критичне погіршення масопереносу.*

Практична цінність. *Виявлене технологічне вікно (5–18 % CO_2) та формалізований енергетичний баланс для тонкостінних структур зі сталі MoNiVa слугують готовим фундаментом для мінімізації геометричних дефектів та максимізації енергоефективності на виробництві. Розроблений алгоритм машинного зору придатний для імплементації в системи керування WAAM із замкненим контуром для предиктивного коригування параметрів у режимі реального часу.*

Ключові слова: *дротове дугове адитивне виробництво, WAAM, холодне перенесення металу, CMT, високоміцна сталь, MoNiVa; захисний газ, питома об'ємна енергія, комп'ютерний зір.*

Список літератури

1. Zhang, H., Li, R., Liu, J., Wang, K., Qiu, W., Shi, L., & et al. (2024). State-of-art review on the process-structure-properties-performance linkage in wire arc additive manufacturing. Virtual and Physical Prototyping, 19(1), e2390495. https://doi.org/10.1080/17452759.2024.2390495

2. Jafari, D., Vaneker, T. H. J., & Gibson, I. (2021). Wire and arc additive manufacturing: Opportunities and challenges to control the quality and accuracy of manufactured parts. Materials & Design, 202, 109471. https://doi.org/10.1016/j.matdes.2021.109471

3. Wang, Y., & Tsai, H. L. (2001). Effects of surface active elements on weld pool fluid flow and weld penetration in gas metal arc welding. Metallurgical and Materials Transactions B, 32, 501–515. https://doi.org/10.1007/s11663-001-0035-5

4. Lu, S., Fujii, H., & Nogi, K. (2004). Marangoni convection and weld shape variations in Ar-O_2 and Ar-CO_2 shielded GTA welding. Materials Science and Engineering: A, 380(1–2), 290–297. https://doi.org/10.1016/j.msea.2004.05.057

5. Wu, F., Falch, K. V., Guo, D., English, P., Drakopoulos, M., & Mirihanage, W. (2020). Time evolved force domination in arc weld pools. Materials & Design, 190, 108534. https://doi.org/10.1016/j.matdes.2020.108534

6. Cunningham, C. R., Flynn, J. M., Shokrani, A., Dhokia, V., & Newman, S. T. (2018). Strategies and processes for high quality wire arc additive manufacturing. Additive Manufacturing, 22, 672–686. https://doi.org/10.1016/j.addma.2018.06.020

7. Kah, P., & Martikainen, J. (2013). Influence of shielding gases in the welding of metals. The International Journal of Advanced Manufacturing Technology, 64 (9–12), 1411–1421. https://doi.org/10.1007/s00170-012-4111-6

8. Teixeira, F. R., Jorge, V. L., Scotti, F. M., Siewert, E., & Scotti, A. (2024). A methodology for shielding-gas selection in wire arc additive manufacturing with stainless steel. Materials, 17(13), 3328. https://doi.org/10.3390/ma17133328

9. Silwal, B., Pudasaini, N., Roy, S., Murphy, A. B., Nycz, A., & Noakes, M. W. (2022). Altering the supply of shielding gases to fabricate distinct geometry in GMA additive manufacturing. Applied Sciences, 12(7), 3679. https://doi.org/10.3390/app12073679

10. Yamaguchi, M., Komata, R., Furumoto, T., Abe, S., & et al. (2022). Influence of metal transfer behavior under Ar and CO_2 shielding gases on geometry and surface roughness of single and multilayer structures in GMAW-based wire arc additive manufacturing of mild steel. The International Journal of Advanced Manufacturing Technology. https://doi.org/10.1007/s00170-021-08231-8

11. Kanishka, K., Acherjee, B., & et al. (2025). A study on the effect of shielding gases on the GMAW-WAAM process and performance of WAAM-deposited low-carbon steel. International Journal of Materials Research. https://doi.org/10.1515/ijmr-2024-0319

12. Akbarzadeh, E., Yurtışık, K., Gür, C. H., & et al. (2024). Influence of shielding gas on the microstructure and mechanical properties of duplex stainless steel in wire arc additive manufacturing. Metals and Materials International, 30(7), 1977–1996. https://doi.org/10.1007/s12540-023-01623-3

13. Marefat, F., Kapil, A., Banaee, S. A., Van Rymenant, P., & Sharma, A. (2023). Evaluating shielding gas-filler wire interaction in bi-metallic wire arc additive manufacturing (WAAM) of creep resistant steel-stainless steel for improved process stability and build quality. Journal of Manufacturing Processes, 88, 110–124. https://doi.org/10.1016/j.jmapro.2023.01.046

14. Yang, G., Deng, F., Zhou, S., Wu, B., Qin, L., & Zheng, J. (2022). Influence of shielding gas nitrogen content on the microstructure and mechanical properties of Cu-reinforced maraging steel fabricated by wire arc additive manufacturing. Materials Science and Engineering: A, 832, 142463. https://doi.org/10.1016/j.msea.2021.142463

15. Rodrigues, T. A., Duarte, V., Avila, J. A., Dias, M. R., Santos, T. G., & Oliveira, J. P. (2019). Wire and arc additive manufacturing of HSLA steel: Effect of thermal cycles on microstructure and mechanical properties. Additive Manufacturing, 27, 440–450. https://doi.org/10.1016/j.addma.2019.03.029

DOI 10.15588/1607-6885-2026-2-10